Phase ordering in nematic liquid crystals

Colin Denniston,[1] Enzo Orlandini,[2] and J. M. Yeomans[3]
[1]*Department of Physics and Astronomy, The Johns Hopkins University, Baltimore, Maryland 21218*
[2]*INFM–Dipartimento di Fisica, Università di Padova, 1-35131 Padova, Italy*
[3]*Department of Physics, Theoretical Physics, University of Oxford, 1 Keble Road, Oxford OX1 3NP, United Kingdom*
(Received 9 January 2001; published 16 July 2001)

We study the kinetics of the nematic-isotropic transition in a two-dimensional liquid crystal by using a lattice Boltzmann scheme that couples the tensor order parameter and the flow consistently. Unlike in previous studies, we find that the time dependences of the correlation function, energy density, and number of topological defects obey dynamic scaling laws with growth exponents that, within the numerical uncertainties, agree with the value 1/2 expected from simple dimensional analysis. We find that these values are not altered by the hydrodynamic flow. In addition, by examining shallow quenches, we find that the presence of orientational disorder can inhibit amplitude ordering.

DOI: 10.1103/PhysRevE.64.021701 PACS number(s): 64.70.Md, 83.80.Xz, 64.60.Ht

I. INTRODUCTION

The phase ordering kinetics of liquid crystal systems undergoing nematic-isotropic transitions has attracted considerable experimental [1–3] and theoretical [4–7] interest. One of the reasons is that nematic liquid crystals provide an experimentally accessible system with continuous symmetry that, unlike systems with discrete symmetry, can display stable topological defects. During phase ordering these defects interact and annihilate and it is believed that many of the universal properties of the late stage kinetic growth can be explained in terms of the defect dynamics. This property is also shared by the well studied $O(N)$ model. However, here the continuous symmetry belongs to a different homotopy class [the $O(N)$ model lacks the inversion symmetry present in the director field of nematic liquid crystals]. It is not yet completely clear if such a difference in the symmetry can modify the ordering dynamics of the nematic liquid crystal.

The aim of this paper is to study the kinetics of phase separation for two-dimensional liquid crystals under a quench from an isotropic to a nematic phase. Considerable controversy exists as to whether the ordering violates dynamical scaling [6]. The simplest scaling analysis based on the assumption of diffusive dynamics for the order parameter suggests that any length scale in the system should grow with a power law in time $t^{1/2}$ [4]. However, an examination of the configuration of the order parameter in experiment (or simulation) clearly shows that the late stage ordering proceeds by defects moving to annihilate. Simple defect arguments that rely on an assumption of a finite constant friction coefficient for the movement of defects also give $t^{1/2}$ [4]. A problem arose due to early calculations [8–10] which showed that the friction coefficient diverges logarithmically with system size. This brought into question whether the $t^{1/2}$ behavior from the simple scaling analysis would be found. Simulations of the XY model [4] and later of tensor models of liquid crystals [6,7] reinforced this view when they failed to measure the $t^{1/2}$ behavior and, in fact, found exponents that appeared to be decreasing away from 1/2 at late times [6]. However, experiments by Pargellis and co-workers [3] found behavior consistent with the $t^{1/2}$ power law. In addition, their simulation of the XY model with very large amplitude noise (considerably larger than that found experimentally) agreed with the $t^{1/2}$ power law. A later more rigorous calculation of the friction coefficient for defect dynamics showed that it does not diverge with system size, but only with vanishing defect velocity [11]. This suggests that it should be possible to measure the $t^{1/2}$ behavior in a simulation.

Another important issue that remains essentially unexplored is the extent to which the presence of hydrodynamic modes coupled to the nematic order parameter can affect the late stage kinetic growth. It is well known that hydrodynamic interactions can crucially influence phase transition kinetics, for example, in simple binary fluid mixtures and in gas-liquid systems [12,13]. In liquid crystals the coupling between the local molecular orientation and the velocity field influences the dynamics of the liquid crystal in a complicated manner. For example, shear flow will cause the molecules to reorient and conversely a reorientation of the liquid crystal may induce a velocity field (backflow). To have a complete picture of the kinetic growth of a phase separating nematic liquid crystal it is crucial to include the effect of these couplings.

Lattice Boltzmann approaches have proved very successful algorithms for investigating phase ordering in binary fluids. Here we use an extension of the method that models liquid crystal hydrodynamics[14,15]. The equations of motion describing liquid crystal hydrodynamics are complex. There are several derivations broadly in agreement, but differing in the detailed form of some terms. Here we follow the approach of Beris and Edwards who write the equations of motion in terms of a tensor order parameter $\mathbf{Q}$ which describes the orientational distribution function of the molecules [16]. This formalism is appropriate here because the motion of defects is explicitly included. Moreover, both the isotropic and nematic phases can be modeled using the same formalism, which is necessary if the dynamics of the transition between them is to be followed.

The paper is organized as follows. In Sec. II we summarize the hydrodynamic equations of motion for liquid crys-

tals. The lattice Boltzmann scheme used to model these equations is described in Sec. III. In Sec. IV we introduce the correlation function, the correlation length, the energy density, and the defect separation as the relevant quantities that characterize the late time behavior of the phase separating system. A review and discussion of previous results is also given. The dynamic scaling behavior of the model is investigated for systems of linear size $L=256$, and the space of the relevant parameters of the model is explored to choose the best values for more computationally intensive simulations. In Sec. V a careful estimate of the dynamical exponents is performed for systems of linear size $L=512$. Numerical results for shallow quenches are presented in Sec. VI. In Sec. VII we make some concluding remarks.

II. THE HYDRODYNAMIC EQUATIONS OF MOTION

There are two major differences between the hydrodynamics of simple liquids and that of liquid crystals. First, the rodlike shape of the molecules means that they are rotated by gradients in the velocity. Second, the equilibrium free energy is more complex than for a simple fluid and this in turn increases the complexity of the stress tensor in the Navier-Stokes equation for the evolution of the fluid momentum. In a general formulation of liquid crystal hydrodynamics [16], the continuum equations of motion are written in terms of a tensor order parameter $\mathbf{Q}$ which is traceless and symmetric and is related to the direction of individual molecules $\vec{m}$ by $Q_{\alpha\beta}=\langle \hat{m}_\alpha \hat{m}_\beta - \frac{1}{3}\delta_{\alpha\beta}\rangle$ where the angular brackets denote a coarse-grained average. (We shall use Greek indices to represent Cartesian directions and assume the usual sum over repeated indices.) The advantage of this approach is that it includes both the isotropic ($\mathbf{Q}=\mathbf{0}$) and the nematic ($\mathbf{Q}\neq\mathbf{0}$) phases and allows an order parameter of variable magnitude within the latter. Hence it is possible to explore the effect of flow on the phase transition between the two states. Moreover the hydrodynamics of topological defects (point defects in two dimensions) is naturally included in the equations. We will study a two-dimensional system with the flow confined to the xy plane. However, we will allow the director field to point in any direction (x, y, and z). As such the tensor order parameter is always a 3×3 matrix.

The equilibrium properties of the liquid crystal are described by the Landau–de Gennes free energy functional [17]

$$\mathcal{F}=\int d^3r\left\{\frac{1}{2}\left(1-\frac{\gamma}{3}\right)Q_{\alpha\beta}^2-\frac{\gamma}{3}Q_{\alpha\beta}Q_{\beta\gamma}Q_{\gamma\alpha}+\frac{\gamma}{4}(Q_{\alpha\beta}^2)^2+\frac{\kappa}{2}(\partial_\alpha Q_{\beta\lambda})^2\right\}. \tag{1}$$

This free energy describes a first-order transition from the isotropic to the nematic phase. In general three elastic constants are needed to fully characterize the nematic phase [17] but we restrict ourselves to a single elastic constant κ. This can be shown to be equivalent to having three equal Frank elastic constants when the order parameter is uniaxial [18]. This simplification is not expected to affect the scaling behavior.

The order parameter $\mathbf{Q}$ is not conserved. It evolves according to a convection-diffusion equation [16,19–21]

$$(\partial_t+\vec{u}\cdot\boldsymbol{\nabla})\mathbf{Q}-\mathbf{S}(\mathbf{W},\mathbf{Q})=\overline{\Gamma}\mathbf{H}, \tag{2}$$

where $\vec{u}$ is the bulk fluid velocity and $\overline{\Gamma}$ is a collective rotational diffusion constant. A generalized form of $\overline{\Gamma}$ is

$$\overline{\Gamma}=\frac{\Gamma}{(1-\frac{3}{2}\mathrm{Tr}\,\mathbf{Q}^2)^2}, \tag{3}$$

where the $\mathbf{Q}$ dependence in the denominator enhances reorientation for well-ordered systems [20]. Note that in previous studies of the kinetics of phase separation for liquid crystals the $\mathbf{Q}$ dependence in the diffusion parameter has always been neglected and $\overline{\Gamma}=\Gamma$ assumed.

The first term on the left-hand side of Eq. (2) is the material derivative describing the usual time dependence of a quantity advected by a fluid with velocity $\vec{u}$. This is generalized by a second term

$$\mathbf{S}(\mathbf{W},\mathbf{Q})=(\mathbf{D}+\boldsymbol{\Omega})(\mathbf{Q}+\mathbf{I}/3)+(\mathbf{Q}+\mathbf{I}/3)(\mathbf{D}-\boldsymbol{\Omega})-2(\mathbf{Q}+\mathbf{I}/3)\mathrm{Tr}(\mathbf{QW}), \tag{4}$$

where $\mathbf{D}=(\mathbf{W}+\mathbf{W}^T)/2$ and $\boldsymbol{\Omega}=(\mathbf{W}-\mathbf{W}^T)/2$ are the symmetric part and the anti-symmetric part, respectively, of the velocity gradient tensor $W_{\alpha\beta}=\partial_\beta u_\alpha$. $\mathbf{S}(\mathbf{W},\mathbf{Q})$ appears in the equations of motion because the order parameter distribution can be both rotated and stretched by flow gradients.

The term on the right-hand side of Eq. (2) describes the relaxation of the order parameter toward the minimum of the free energy in a way analogous to model A [22]. The molecular field $\mathbf{H}$ that provides the driving motion is related to the derivative of the free energy by

$$\mathbf{H}=-\frac{\delta\mathcal{F}}{\delta\mathbf{Q}}+(\mathbf{I}/3)\mathrm{Tr}\left\{\frac{\delta\mathcal{F}}{\delta\mathbf{Q}}\right\}. \tag{5}$$

The flow of the liquid crystal of density ρ obeys the continuity equation

$$\partial_t\rho+\partial_\alpha\rho u_\alpha=0 \tag{6}$$

and the Navier-Stokes equation

$$\rho\partial_t u_\alpha+\rho u_\beta\partial_\beta u_\alpha=\partial_\beta\tau_{\alpha\beta}+\partial_\beta\sigma_{\alpha\beta}+\frac{\rho\tau_f}{3}\times\partial_\beta[(1-3\partial_\rho P_0)\delta_{\alpha\beta}\partial_\gamma u_\gamma+\partial_\alpha u_\beta+\partial_\beta u_\alpha] \tag{7}$$

where τ_f is related to the viscosity and P_0 is the pressure,

$$P_0=\rho T-\frac{\kappa}{2}(\boldsymbol{\nabla}\mathbf{Q})^2. \tag{8}$$

The details of the stress tensor reflect the additional complications of liquid crystal hydrodynamics with respect to simple fluids. There is a symmetric contribution

$$\sigma_{\alpha\beta} = -P_0\delta_{\alpha\beta} - 3H_{\alpha\beta} - \partial_\beta Q_{\gamma\nu}\frac{\delta\mathcal{F}}{\delta\partial_\alpha Q_{\gamma\nu}} \tag{9}$$

and an antisymmetric contribution

$$\tau_{\alpha\beta} = Q_{\alpha\gamma}H_{\gamma\beta} - H_{\alpha\gamma}Q_{\gamma\beta}. \tag{10}$$

For the symmetric contribution we are using the form derived by Doi [20]. This is only quantitatively correct in the vicinity of the transition with the general form being slightly more complex [16]. We do not expect any qualitative differences to result from this difference in the regime in which we operate in this paper.

III. A LATTICE BOLTZMANN ALGORITHM FOR LIQUID CRYSTAL HYDRODYNAMICS

We now define a lattice Boltzmann algorithm that solves the hydrodynamic equations of motion of a liquid crystal (2), (6), and (7). This section may safely be omitted by readers interested in the physical results but not in the details of the simulations.

Lattice Boltzmann algorithms are defined in terms of a set of continuous variables, usefully termed partial distribution functions, which move on a lattice in discrete space and time [23]. The simplest lattice Boltzmann algorithm, which describes the Navier-Stokes equations of a simple fluid, is defined in terms of a single set of partial distribution functions that sum on each site to give the density. For liquid crystal hydrodynamics this must be supplemented by a second set, which are tensor variables, and which are related to the tensor order parameter **Q**.

We define two distribution functions, the scalars $f_i(\vec{x})$ and the symmetric traceless tensors $\mathbf{G}_i(\vec{x})$, on each lattice site $\vec{x}$. Each $f_i, \mathbf{G}_i$ is associated with a lattice vector $\vec{e}_i$. We choose a nine-velocity model on a square lattice with velocity vectors $\vec{e}_i = (\pm 1,0),(0,\pm 1),(\pm 1,\pm 1),(0,0)$. Physical variables are defined as moments of the distribution function

$$\rho = \sum_i f_i, \quad \rho u_\alpha = \sum_i f_i e_{i\alpha}, \quad \mathbf{Q} = \sum_i \mathbf{G}_i. \tag{11}$$

The distribution functions evolve in a time step Δt according to

$$f_i(\vec{x}+\vec{e}_i\Delta t, t+\Delta t) - f_i(\vec{x},t) = \frac{\Delta t}{2}[\mathcal{C}_{f_i}(\vec{x},t,\{f_i\}) + \mathcal{C}_{f_i}(\vec{x}+\vec{e}_i\Delta t, t+\Delta t, \{f_i^*\})], \tag{12}$$

$$\mathbf{G}_i(\vec{x}+\vec{e}_i\Delta t, t+\Delta t) - \mathbf{G}_i(\vec{x},t) = \frac{\Delta t}{2}[\mathcal{C}_{\mathbf{G}_i}(\vec{x},t,\{\mathbf{G}_i\}) + \mathcal{C}_{\mathbf{G}_i}(\vec{x}+\vec{e}_i\Delta t, t+\Delta t, \{\mathbf{G}_i^*\})]. \tag{13}$$

The left-hand side of these equations represents free streaming with velocity $\vec{e}_i$, while the right-hand side is a collision step which allows the distribution to relax toward equilibrium. f_i^* and $\mathbf{G}_i^*$ are first-order approximations to $f_i(\vec{x}+\vec{e}_i\Delta t, t+\Delta t)$ and $\mathbf{G}_i(\vec{x}+\vec{e}_i\Delta t, t+\Delta t)$, respectively. They are obtained from Eqs. (12) and (13) but with f_i^* and $\mathbf{G}_i^*$ set to f_i and $\mathbf{G}_i$. Discretizing in this way, which is similar to a predictor-corrector scheme, has the advantages that lattice viscosity terms are eliminated to second order and that the stability of the scheme is improved.

The collision operators are taken to have the form of a single relaxation time Boltzmann equation, together with a forcing term

$$\mathcal{C}_{f_i}(\vec{x},t,\{f_i\}) = -\frac{1}{\tau_f}[f_i(\vec{x},t) - f_i^{eq}(\vec{x},t,\{f_i\})] + p_i(\vec{x},t,\{f_i\}), \tag{14}$$

$$\mathcal{C}_{\mathbf{G}_i}(\vec{x},t,\{\mathbf{G}_i\}) = -\frac{1}{\tau_{\mathbf{G}}}[\mathbf{G}_i(\vec{x},t) - \mathbf{G}_i^{eq}(\vec{x},t,\{\mathbf{G}_i\})] + \mathbf{M}_i(\vec{x},t,\{\mathbf{G}_i\}). \tag{15}$$

The form of the equations of motion and thermodynamic equilibrium follow from the choice of the moments of the equilibrium distributions f_i^{eq} and $\mathbf{G}_i^{eq}$ and the driving terms p_i and $\mathbf{M}_i$. f_i^{eq} is constrained by

$$\sum_i f_i^{eq} = \rho, \quad \sum_i f_i^{eq} e_{i\alpha} = \rho u_\alpha,$$

$$\sum_i f_i^{eq} e_{i\alpha} e_{i\beta} = -\sigma_{\alpha\beta} + \rho u_\alpha u_\beta, \tag{16}$$

where the zeroth and first moments are chosen to impose conservation of mass and momentum. The second moment of f^{eq} controls the symmetric part of the stress tensor, whereas the moments of p_i

$$\sum_i p_i = 0, \quad \sum_i p_i e_{i\alpha} = \partial_\beta \tau_{\alpha\beta}, \quad \sum_i p_i e_{i\alpha} e_{i\beta} = 0 \tag{17}$$

impose the antisymmetric part of the stress tensor. For the equilibrium of the order parameter distribution we choose

$$\sum_i \mathbf{G}_i^{eq} = \mathbf{Q}, \quad \sum_i \mathbf{G}_i^{eq} e_{i\alpha} = \mathbf{Q}u_\alpha,$$

$$\sum_i \mathbf{G}_i^{eq} e_{i\alpha} e_{i\beta} = \mathbf{Q}u_\alpha u_\beta. \tag{18}$$

This ensures that the order parameter is convected with the flow. Finally, the evolution of the order parameter is most conveniently modeled by choosing

$$\sum_i \mathbf{M}_i = \bar{\Gamma}\mathbf{H}(\mathbf{Q}) + \mathbf{S}(\mathbf{W},\mathbf{Q}), \quad \sum_i \mathbf{M}_i e_{i\alpha} = \left(\sum_i \mathbf{M}_i\right) u_\alpha, \tag{19}$$

which ensures that the fluid minimizes its free energy at equilibrium.

Conditions (16)–(19) can be satisfied as is usual in lattice Boltzmann schemes by writing the equilibrium distribution functions and forcing terms as polynomial expansions in the velocity [23]. Taking the continuum limit of Eqs. (12) and (13) and performing a Chapman-Enskog expansion leads to the equations of motion of liquid crystal hydrodynamics (2), (6), and (7) [14].

IV. PHASE ORDERING KINETICS

A. Measures

The kinetics of phase separation in liquid crystals has been examined using simulations by Zapotocky *et al.* [6] and more recently by Fukuda [7]. The former studied phase separation in the diffusive regime while the latter added hydrodynamics. In both cases, rather deep quenches were performed and three different quantities considered in order to make a quantitative analysis of the domain growth.

The first measure is the scalar correlation function for the tensorial nematic order parameter $\mathbf{Q}$ defined by [6]

$$C(\mathbf{r},t) = \frac{\langle \mathrm{Tr}[\mathbf{Q}(\mathbf{0},t)\mathbf{Q}(\mathbf{r},t)]\rangle}{\langle \mathrm{Tr}\,\mathbf{Q}^2(\mathbf{0},t)\rangle}, \tag{20}$$

where $\langle\cdots\rangle$ denotes averaging over the positions $\mathbf{0}$. The correlation function is normalized so that $C(\mathbf{0},t)=1$. A correlation length $L_{cor}(t)$ at time t is defined by

$$C(L_{cor},t) = 1/2. \tag{21}$$

Dynamical scaling states that the system is dynamically self-similar in time, except for a change in the length scale. If dynamical scaling holds, the correlation length will control the statistical properties of the system. Plotting the correlation function as a function of $\mathbf{r}/L_{cor}(t)$, the data at different times should collapse onto a single curve. Moreover, $L_{cor}(t)$ should decay with time as a power law

$$L_{cor}(t) \sim t^{\phi_{cor}}. \tag{22}$$

Zapotocky *et al.* [6] obtained an exponent $\phi_{cor}=0.41$ significantly lower than the value 1/2 suggested by the diffusive character of the equation of motion for the order parameter (2) and by scaling arguments [24].

A second measure is the Fourier transform of the correlation function, the structure factor $S(k,t)$. The scaling form for the structure factor in d dimensions is

$$S(k,t) = L_{cor}^d(t)\, g(kL_{cor}(t)) \tag{23}$$

where g should have the form $g(y)\sim y^{-(N+d)}$ for large y for the $O(N)$ vector model (Porod's law) [25]. To see how this arises note that, for $y=kL_{cor}\gg 1$, the structure factor probes the order parameter at length scales much smaller than the separation between defects. Substantial variation of the order parameter on these length scales happens only in the vicinity of the defect cores, and is not related to interdefect correlations. This implies that

$$S(k,t) \sim \rho_{def}(t)\, b(k), \quad kL_{cor}\gg 1, \tag{24}$$

where ρ_{def} is the density of defects in the system and $b(k)$ is a function of k only. If we further assume that the separation of defects scales as the correlation length L_{cor}, so that $\rho_{def} \propto L_{cor}(t)^{-(d-s)}$, where s is the dimensionality of the defect (zero here), then for $d=2$ scaling implies

$$g(y) \sim y^{-[d+(d-s)]} = y^{-4}. \tag{25}$$

Zapotocky and collaborators did find the y^{-4} behavior in the tails [6]. They also noted that the scaling functions appeared to approach the y^{-4} law from above. This effect has been observed experimentally and it is attributed to interdefect correlations.

A scaling form also holds for the elastic energy. To see this note from Eq. (1) that

$$\mathcal{F}_{el} \propto \int d\mathbf{r}(\partial_\alpha Q_{\beta\gamma})(\partial_\alpha Q_{\beta\gamma}) = \int d\mathbf{k} k^2 S(k,t)$$
$$= \int d\mathbf{k}[kL_{cor}(t)]^2 g(kL_{cor}(t)) \tag{26}$$

for $d=2$ where the last line has been obtained by using the scaling form Eq. (23). The integral can be split into three parts, $0<r<a$, $a<r<L_{cor}(t)$, and $L_{cor}(t)<r<\infty$, where a is a cutoff. Assuming that the result is not dependent on the cutoff, the first part can be neglected, whereas for the second contribution using Porod's law for g and integrating from a to $L_{cor}(t)$ gives

$$\mathcal{F}_{el} \propto L_{cor}(t)^{-2} \ln[L_{cor}(t)/a]. \tag{27}$$

The last term can be neglected since it should scale roughly as $L_{cor}^{-2}(t)$ assuming that $g(y)$ is approximately constant at small y. Differentiating Eq. (27),

$$\frac{d\ln\mathcal{F}_{el}}{d\ln t} = \frac{d\ln L_{cor}(t)}{d\ln t}\frac{d\ln\mathcal{F}_{el}}{d\ln L_{cor}}$$
$$\sim \phi_{cor}(t)\left(-2 + \frac{1}{\ln[L_{cor}(t)/a]}\right), \tag{28}$$

where $\phi_{cor}(t)$ is the exponent from the scaling of the correlation length. We define a new exponent for the characteristic energy as

$$\phi_{el}(t) = -\frac{1}{2}\frac{d\ln\mathcal{F}_{el}}{d\ln t} \sim \phi_{cor}(t) - \frac{\phi_{cor}(t)}{2\ln[L_{cor}(t)/a]}. \tag{29}$$

Note the logarithmic corrections to the scaling of the elastic energy. Taking these into account, Zapotocky *et al.* obtained reasonable agreement between ϕ_{el} and ϕ_{cor}, whereas without taking them into account they obtained $\phi_{el}=0.325 < \phi_{cor}$ [6].

A length scale can also be obtained from the average separation of topological defects. This separation is found by counting the number of defects in the system to obtain ρ_{def} and then taking

$$L_{def}(t)=1/\sqrt{\rho_{def}}. \tag{30}$$

Zapotocky *et al.* obtained a value $\phi_{def}=0.374$ for the corresponding exponent. It is assumed that defect annihilation is the process that controls the growth of the correlation length and therefore dynamical scaling implies $\phi_{cor}=\phi_{def}$. Zapotocky *et al.* could give no explanation of the discrepancy in their values and interpreted it as an indication of the violation of dynamical scaling.

Indeed, in almost all of the published numerical work on phase ordering in systems that order via the annihilation of topological defects, it has been found that the exponents are less than the value 1/2 expected from dimensional analysis. A suggestive argument for the origin of this discrepancy has been given by Yurke *et al.* [5] for the $O(2)$ model. These authors obtained an approximate equation of motion for an isolated defect-antidefect pair by equating the attractive and frictional forces acting on each defect. The attractive force was assumed to have the form $F_{at} \propto -1/L$ where L is the separation of the defects. This would seem to be a reasonable assumption as it is well known that the energy of such a pair varies as $\ln L$ [17]. The frictional force was taken to be $F_{fr} \propto v \ln(R/a)$ where R is the ''size'' of a defect, a its core size, and $v=\frac{1}{2}dL/dt$ its velocity. The ''size'' is then assumed to be equal to L. Assigning a defect size of L may seem somewhat questionable. However, the assumption can be supported by a more rigorous argument [11].

Equating the frictional and elastic forces gives an implicit formula for the defect separation as a function of the time t before annihilation,

$$L_{def}(t) \sim \left[\frac{t}{\ln[L_{def}(t)/a]-1/2} \right]^{1/2}. \tag{31}$$

The growth in this length scale for increasing times before annihilation is then assumed to be the same as the growth in the average separation of defects after a quench. This gives an apparent exponent

$$\phi_{def} \propto \frac{1}{2}\left[\frac{t}{L_{def}^2(t)\ln[L_{def}(t)/a]} \right]. \tag{32}$$

The argument implies that the failure to measure $t^{1/2}$ is due to logarithmic corrections. However, it has been claimed [6] that this is effectively untestable because of the unknown constant of proportionality in Eq. (32). One can, however, measure an effective exponent for the two-defect case and compare it to that for the average separation after a quench. Zapotocky *et al.* obtained a similar value, $\phi_{def}=0.375$ [6].

More recently Fukuda [7] has investigated the effect of the stress-induced flow on the kinetics of the nematic-isotropic transition by numerically solving the hydrodynamic equations for the tensor order parameter **Q** and the fluid velocity in $d=2$. The equations of motion were slightly different from the ones considered here. An older model that considers a corotational derivative rather than an upper convective derivative [26] was used. For the purely dissipative case Fukuda obtained similar exponents to Zapotocky *et al.*; for the hydrodynamic case he obtained $\phi_{cor} \simeq \phi_{def} = 0.43$. Note that, in contrast to the case without flow, $\phi_{cor} \simeq \phi_{def}$, indicating that the dynamical scaling hypothesis is confirmed when hydrodynamics is included. However, the value calculated is still lower than the value 1/2 expected for these systems.

Most experiments on phase ordering in liquid crystals are in the three-dimensional regime where the defect line energy controls the dynamics. There are only a limited number of experiments in a two-dimensional geometry [27,3]. Even in the experiments it is difficult to reach the asymptotic regime and the expected power law of t^{-1} for the number of defects is only obtained for the last decade of time [3].

B. Corrections to scaling and parameter space

Our goal is to ascertain why previous studies have not measured the expected exponents and then, if possible, to perform simulations in the asymptotic scaling regime to obtain precise exponent values. In order to do this we first determine numerically the dependence of the corrections to scaling on the parameters at our disposal. In doing this we will see that the difficulty in obtaining the asymptotic values of the exponents may have had as much to do with the fine scale details of the simulation on the lattice as with the constraints of lattice size and run times.

As it seems clear from all previous studies that the phase behavior is dominated by the motion of **Q** in the plane, we restrict the order parameter to be of the form

$$\mathbf{Q}=\begin{pmatrix} Q_{xx} & Q_{xy} & 0 \\ Q_{xy} & Q_{yy} & 0 \\ 0 & 0 & -(Q_{xx}+Q_{yy}) \end{pmatrix}, \tag{33}$$

in order to speed up the numerics. The quenches that we consider are envisaged to start at a high temperature, at which the equilibrium phase is the disordered, isotropic phase. We take as the initial condition for the lattice Boltzmann simulations a configuration representative of this phase in which the $Q_{\alpha\beta}$ at each lattice point are random numbers uniformly distributed in a small interval $[-\delta,\delta]$. More precisely, by writing

$$Q_{xx}=A(3\cos\phi\cos\phi-1)/2,$$

$$Q_{xy}=3A\cos\phi\sin\phi/2,$$

$$Q_{yy}=A(3\sin\phi\sin\phi-1)/2, \tag{34}$$

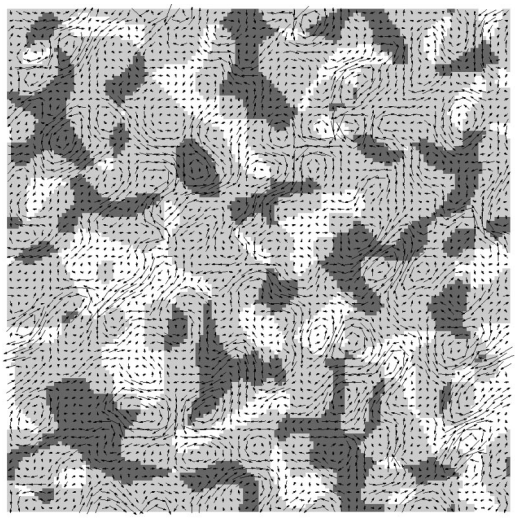

FIG. 1. Schlieren pattern (shading) and fluid velocity (vectors) associated with the ordering of a liquid crystal after a quench from the isotropic to the nematic phase. The director in the darkest regions is perpendicular to the director in the lightest regions (with the other shade in between). The shading on the Schlieren pattern has been rendered with only three shades of gray so as not to obscure the vector field. Disclinations of strength $\pm 1/2$ are located at the intersection of dark gray and white "brushes."

the initial configuration is obtained by assigning, at each lattice point, a random number in the range $[-0.02,0.02]$ for the amplitude A and a random number in $[-\pi,\pi]$ for the phase ϕ.

To ascertain a rough dependence of the corrections to scaling on the various parameters of the system we examined quenches below and close to the spinodal line for several sets of parameters values. For this exploration of parameter space we used a lattice size of 256×256 and averaged over only two to five runs.

Figure 1 shows the Schlieren pattern and associated fluid flow from a typical run. The shading indicates the orientation of the director field and the arrows the fluid velocity. The thing to note in such a diagram is the intersection of light and dark "brushes," which indicate the location of the $\pm 1/2$ disclinations. It is apparent that the main features of the flow are the vortices associated with the moving disclinations. The interaction of vortices in two-dimensional flow has the same form as the interaction of disclinations in the director field so one does not expect any qualitative changes in the scaling behavior.

We now compare five sets of data. The first four data sets are a quench to $\gamma=3.25$ (note that the first-order transition is at $\gamma=2.7$ and that the spinodal is at $\gamma=3.0$). The first is a baseline run. In the second $\overline{\Gamma}$ is given by Eq. (3) whereas in the others $\overline{\Gamma}$ is taken to be a constant and equal to 1. In the third we turn off hydrodynamics by relaxing the momentum conservation constraint [i.e., the second equation in (16)] at time $t=5000$. The fourth has a value of κ ten times smaller than the rest. The fifth data set is similar to the first except now the quench is deeper, to $\gamma=3.7$.

The correlation function for $\gamma=3.25$ and with the renormalized diffusion constant is shown in Fig. 2. There is a reasonable collapse of the data when the correlation function is plotted against $r/L_{cor}(t)$. This is as expected from dynamical scaling. However, even if a function does appear to collapse it is very hard to measure the quality of the collapse and hence this provides only a weak test of scaling.

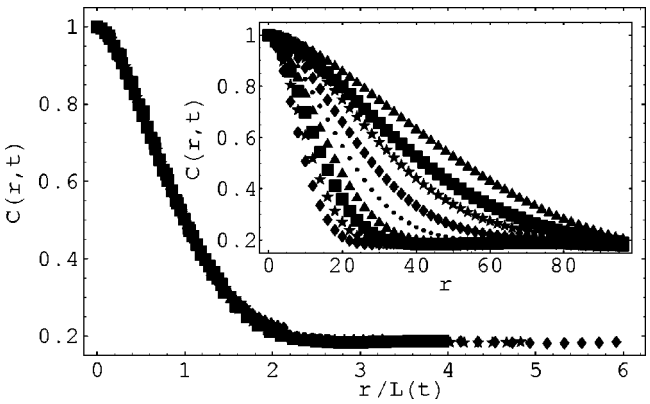

FIG. 2. Correlation function for $\gamma=3.25$ and with renormalized diffusion constant. Inset: unscaled correlation function for times between $t=159$ and 8913. Main figure: correlation function as a function of $r/L(t)$ where $L(t)$ is determined as the length at which the unscaled correlation function crosses 1/2.

Figure 3 shows the length scale obtained from the correlation function L_{cor} as a function of time for all five data sets. The exponents $\phi_{cor},\phi_{def},\phi_{el}$ obtained by fitting these data, as well as similar data for the number of defects and the distortion energy, to power laws are given in Table I. Although, as there are corrections to scaling, this is not a good way of obtaining the exponents, it does allow for a clear comparison between the different parameter sets. A more sophisticated way of estimating the growth exponents is to obtain an effective exponent $\phi(t^*)$ by performing a simple linear fit to the plots of $\ln L$ versus $\ln t$ (e.g., Fig. 3) for data

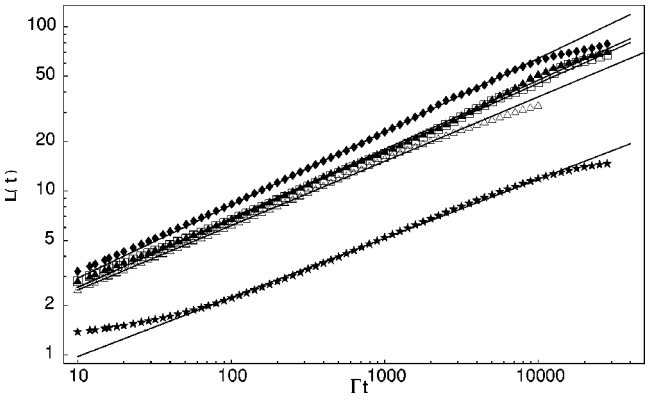

FIG. 3. Length scale obtained from scaling of correlation function as a function of time. The lines are power law fits and the symbols correspond to box, $\gamma=3.25$, baseline; diamond, $\gamma=3.25$, renormalized diffusion constant; filled triangle, $\gamma=3.25$, hydrodynamics off; star, $\gamma=3.25$, small κ; hollow triangle, $\gamma=3.7$ as baseline. In this figure (and all others) times are multiplied by Γ to make them dimensionless and distances are measured in units of the lattice spacing of the simulation.

TABLE I. Comparison of the exponents obtained by fitting the data from runs on small systems (e.g., below Fig. 4) to a power law. The statistical errors ~ 0.003 and the systematic errors ~ 0.015 (as the end points of the fit are changed).

Run	Parameter set	Exponents		
		ϕ_{cor}	ϕ_{def}	ϕ_d
Baseline	$\gamma=3.25,\ \overline{\Gamma}=1,\ \kappa=0.02$	0.42	0.406	0.35
Renorm. diffusion	$\gamma=3.25,\ \overline{\Gamma}=(1-\frac{3}{2}\mathrm{Tr}\,\mathbf{Q}^2)^{-2},\ \kappa=0.02$	0.45	0.43	0.365
No hydrodynamics	$\gamma=3.25,\ \overline{\Gamma}=1,\ \kappa=0.02$	0.42	0.398	0.345
More localized defects	$\gamma=3.25,\ \overline{\Gamma}=1,\ \kappa=0.002$	0.36	0.33	0.27
Deeper quench	$\gamma=3.7,\ \overline{\Gamma}=1,\ \kappa=0.02$	0.39	0.36	0.31

in the interval $t_{-m},t_{-m+1},\ldots,t^*,\ldots,t_{m-1},t_m$. $m=8$ is used in the fits presented here.

From these preliminary runs with $L=256$ we can make the following observations.

(1) A renormalized diffusion constant $\overline{\Gamma}$ seems to help in the sense that the exponents are closer to the expected asymptotic value of 1/2. However this turns out to be mostly an early time effect. To see this we plot the effective correlation length exponent as a function of time in Fig. 4 for the first two data sets in Table I. We see that for the baseline data set the exponent first decreases and then increases with time whereas with the renormalized diffusion constant $\overline{\Gamma}$ the exponent immediately starts increasing with time toward the asymptotic value. Thus, we are effectively accessing longer times with the renormalized diffusion constant. This is reasonable because the initial ordering in the system, where the order parameter saturates away from the defect cores, is a diffusive process.

(2) Hydrodynamics appears to speed the ordering very slightly, but not by a significant amount. The crucial test here is the run denoted in Fig. 3 by filled triangles where at a given time step ($t=5000$) we have explicitly switched off the hydrodynamics by randomizing the velocity directions after each collision step. One can see in Fig. 3 that no significant change occurs with respect to the run in which the hydrodynamics is fully taken into account. This conclusion agrees with previous results by Fukuda [7] even though his formulation of the model is somewhat different from ours.

(3) Reducing κ reduces the size of the defect cores and we find that changing κ has a significant effect on the results.

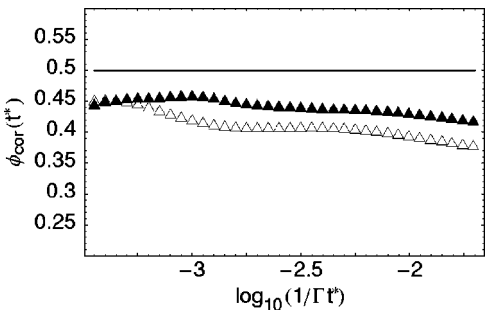

FIG. 4. Effective exponent for the growth of the correlation length as a function of time. Empty triangle, $\gamma=3.25$, baseline; filled triangle, $\gamma=3.25$, renormalized diffusion constant.

To see this we compare results for the baseline run with $\kappa=0.02$ to the run with a value of κ ten times smaller ($\kappa=0.002$). The effective exponent extracted from the correlation function is shown in Fig. 5. There are a few important things to note from this figure. First the effective exponent is not a monotonic function of time: it reaches a maximum value at a given time and then it decreases as time is further increased. This is true for the baseline case as well, but the time at which it happens is much larger than for the run with more localized defects. Note that this effect has also been observed in previous simulations [6] and interpreted as the onset of freezing in the dynamics, due mainly to the finite size of the system simulated. However, the fact that the effect is stronger for smaller values of κ suggests instead a lattice discretization effect.

As an obvious length scale in this problem is the size of a defect core a it is tempting to take κ as small as possible to minimize this scale. However, once a defect core is of the order of a lattice spacing, it becomes energetically advantageous for a defect to be centered in a plaquette of the lattice as this will minimize the distortion in the amplitude of the order parameter that is actually realized on the lattice, as shown in Fig. 6. This creates an additional potential which can trap the defect. The height of this potential is a decreasing function of κ as, if the amplitude distortion caused by a defect is spread over many sites, the defect will be less sensitive to exactly where it is centered.

This effect occurs at later times in the simulation because

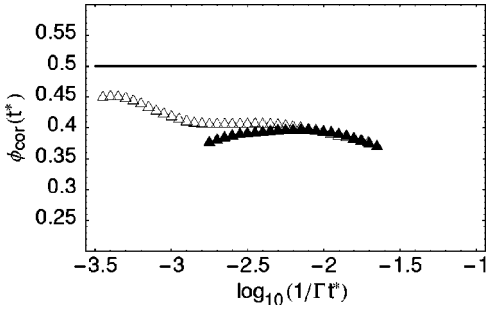

FIG. 5. Effective exponent for the growth of the correlation length as a function of time. Empty triangle, $\gamma=3.25$, baseline; filled triangle, $\gamma=3.25$, $\kappa=1/10$ of the baseline value. The time t^* has been multiplied by 1/10 (i.e., time is scaled by $1/\kappa$) for the small κ case.

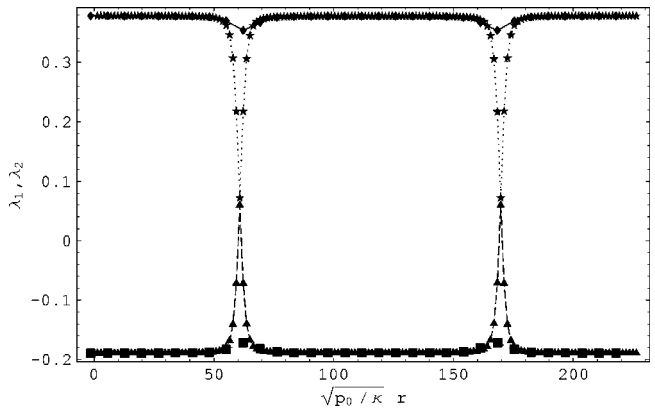

FIG. 6. Two largest eigenvalues of **Q** along a cut joining the center of two $\pm 1/2$ defects moving to annihilate each other. The squares and diamonds are for the case with $\kappa=0.02$ and the stars and triangles for $\kappa=0.5$. The dips are an indication of the lattice pinning potential. The abscissa is scaled by the length $\sqrt{\kappa/p_0}$ to make it dimensionless (all other parameters are the same).

interdefect interactions decrease as the defect spacing increases. At the point where the lattice pinning potential balances the defect-defect interactions motion will stop. Indeed, even before this time, the lattice pinning will cause an additional frictional drag on the defects, which could be detrimental in trying to fit to theory. Thus we see that taking κ small to try to achieve longer length scales (as appears to have been done in almost all previous work) is a trap better avoided.

Second, as can be seen from Fig. 5 , if the time is scaled by κ the effective exponent for the baseline case appears to continue on the same curve as for smaller κ. At first this seems surprising since one might expect time to scale with the diffusion constant, but not necessarily with κ. To see why it occurs one can substitute a form for the director of a uniaxial nematic away from the defect core, $\mathbf{n}=(\cos\theta, \sin\theta)$, into Eq. (2). Ignoring the hydrodynamic flow one obtains a diffusion equation for θ,

$$\partial_t \theta = D_\theta \nabla^2 \theta, \tag{35}$$

where $D_\theta = \kappa\overline{\Gamma}$, confirming that the relevant diffusion constant is proportional to both $\overline{\Gamma}$ and κ [15,11].

(4) Finally, the data for deeper quenches show an exponent further from 1/2. This is also due to the pinning potential described above. As can be seen from the effective exponents shown in Fig. 7 the freezing happens at an earlier time for the deeper quench. This is not surprising as defects are more localized further from the transition and hence the lattice pinning potential will be greater.

V. ASYMPTOTIC RESULTS: CRITICAL EXPONENTS

In the previous section we examined the kinetics of phase ordering in a system of linear size $L=256$ averaging over only a few initial configurations. This allowed us to explore in a more systematic way the space of the parameters (i.e., γ, $\kappa, \overline{\Gamma}$) relevant to the kinetics. In particular, we found that by

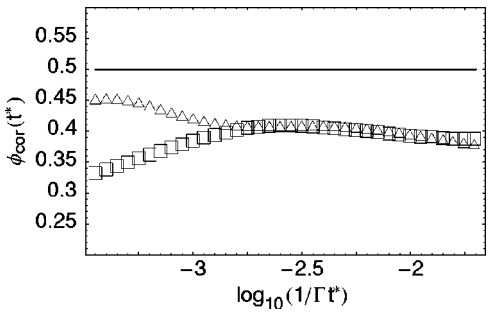

FIG. 7. Effective exponent for the growth of the correlation length as a function of time. Triangle, $\gamma=3.25$, baseline; box, $\gamma=3.7$, baseline.

using a renormalized diffusion constant $\overline{\Gamma}$ and values of κ big enough to avoid pinning effects better scaling behavior is achieved in less time. Using this knowledge we now simulate bigger systems and average over more starting configurations to obtain more precise results for the dynamical critical exponents of the model.

We focus on the scaling behavior of the correlation function, the average defect separation, and the elastic energy for phase separating systems of linear size $L=512$. Averages were taken over 20 initial configurations. Quenches were run for $\gamma=3.25$ and $\gamma=3.0$. In both cases $\kappa=0.3$ and $\overline{\Gamma}=1/(1-\frac{3}{2}\,\mathrm{Tr}\,\mathbf{Q}^2)^2$.

Figure 8 shows the time evolution of the length scale obtained from the correlation function for the two data sets. Note that at late times the data (on the log-log plot) display a linear behavior with slope close to 1/2. A simple linear fit of the data with $t \geqslant t_x = 2239$ gives

$$\phi_{cor} = 0.50 \pm 0.01 \tag{36}$$

for $\gamma=3.25$, and

$$\phi_{cor} = 0.48 \pm 0.02 \tag{37}$$

for $\gamma=3.00$. The errors were obtained by varying t_x between 502 and 5012. This systematic error was much more significant than statistical errors evaluated from the χ^2 statistics of the linear fit.

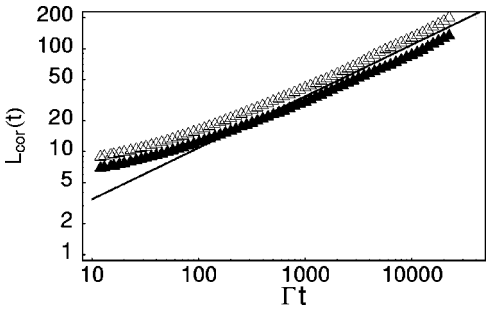

FIG. 8. Length scale obtained from the correlation function as a function of time. The line is a guide to the eye and has slope 1/2. The symbols correspond to empty triangle, $\gamma=3.25$, and filled triangle, $\gamma=3.00$.

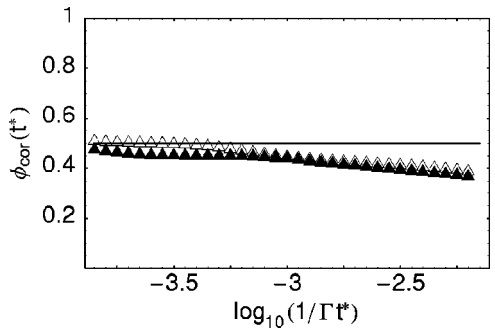

FIG. 9. Effective exponent for the growth of the correlation length as a function of time. Filled triangle, $\gamma=3.00$; empty triangle, $\gamma=3.25$.

As we have argued in the previous section a better quantity to check is the effective exponent $\phi(t^*)$ as a function of fitting time t^*. In Fig. 9 we show the effective exponent for the correlation length $\phi_{cor}(t^*)$ as a function of inverse time. Note that the asymptotic value of 1/2 is clearly reached for the last decade in time. As far as we know this is the first time that strong evidence has been obtained for the conjectured 1/2 dynamical exponent for a phase separating nematic liquid crystal.

Similar plots for the effective exponent for the number of defects $\phi_{def}(t^*)$ are shown in Fig. 10. By looking at the high t^* behavior we obtain

$$\phi_{def}=0.47\pm0.03 \quad \text{for} \quad \gamma=3.25,$$

$$\phi_{def}=0.48\pm0.03 \quad \text{for} \quad \gamma=3.00, \tag{38}$$

where the errors have been estimated from the fluctuations in the effective exponents from a moving average with fewer points (four in this case). Again, we see that the asymptotic value of the exponent is consistent with 1/2.

Finally, Fig. 11(a) shows the exponent obtained from the elastic energy $\phi_{el}(t^*)$. In this case a simple linear fit produces an asymptotic value smaller than 1/2 (~ 0.4 in the plot). This is mainly due to the logarithmic corrections to the scaling of the elastic energy [Eq. (27)] which depress the effective growth exponent for the characteristic energy length with respect to the correlation length exponent [Eq. (29)]. Indeed, by adding the logarithmic corrections to scaling as in Eq. (29), we can bring the exponent into agreement with that obtained from the correlation function, as shown in Fig. 11(b).

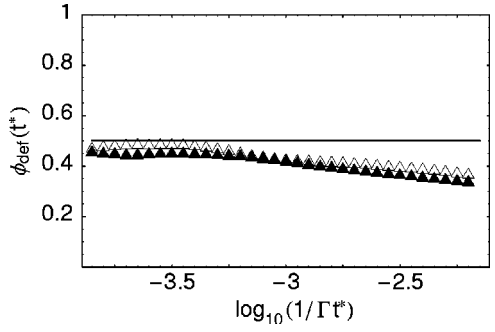

FIG. 10. Effective exponent for the growth of the defect separation length as a function of time. Filled triangle, $\gamma=3.00$; empty triangle, $\gamma=3.25$.

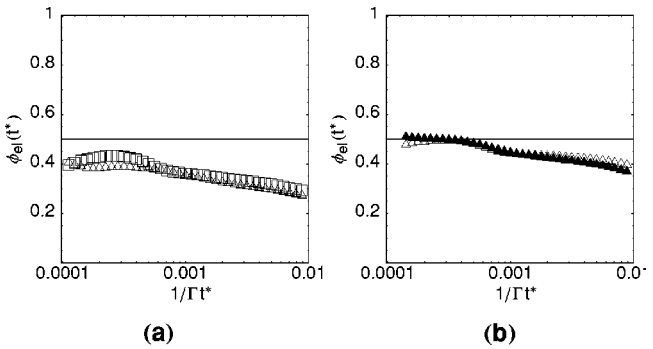

FIG. 11. (a) Effective exponent for the growth of the elastic energy length as a function of time triangle, $\gamma=3.00$; box, $\gamma=3.25$. (b) Effective exponent for the correlation length (filled triangle), and the growth of the elastic energy corrected for the logarithmic scaling of Eq. (29) (empty triangle).

By extrapolating the effective exponents at high t^* values we obtain,

$$\phi_{el}=0.47\pm0.03 \quad \text{for} \quad \gamma=3.25,$$

$$\phi_{el}=0.50\pm0.03 \quad \text{for} \quad \gamma=3.00. \tag{39}$$

VI. SHALLOW QUENCHES

So far, we have examined the late stage kinetics of the orientational ordering, long after the amplitude has ordered. In this regime, the ordering has shown dynamics consistent with that expected for a diffusive XY model. It is also interesting to examine the early stage dynamics and shallower quenches where one may observe an interaction between the two symmetries of the problem [i.e., those of the scalar order parameter and the essentially $O(2)$ symmetry of the orientational order].

First we examine what is naively expected for the amplitude ordering dynamics. Assuming that the orientational degrees of freedom are completely ordered the free energy can be written in terms of just the amplitude of the order parameter q [20],

$$\mathcal{F}=\frac{1}{2}\left(1-\frac{\gamma}{3}\right)q^2-\frac{\gamma}{9}q^3+\frac{\gamma}{6}q^4. \tag{40}$$

This is shown as the solid curves in Fig. 12 for the cases $\gamma=2.7$ (phase transition point) and $\gamma=3.0$ (spinodal line, where the barrier between the isotropic and nematic states vanishes). One expects the presence of a free energy barrier between the isotropic and nematic states to affect the phase ordering dynamics. In the presence of a barrier a finite region of the nematic phase must be nucleated to initiate growth. Beyond the spinodal (which occurs at $\gamma=3.0$) the system will order spontaneously by spinodal decomposition throughout space. If we artificially orient the director field before quenching, this is indeed what is observed.

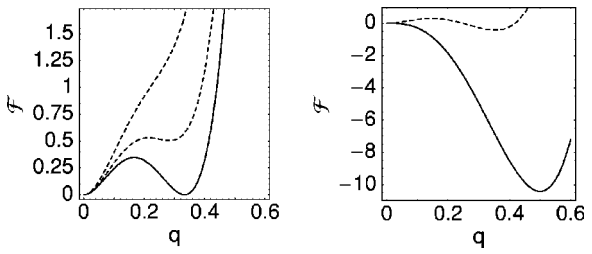

FIG. 12. Free energy ($\times 10^3$) versus magnitude of the order parameter q for $\gamma=2.7$ (left) and $\gamma=3.0$ (right). Solid lines correspond to the assumption of complete orientational order and dashed lines correspond to the spatially averaged free energy for different values of the defect separation (6 and 12 in left figure and 2 in right figure).

However, in a normal quench where the director is not oriented, one observes somewhat different behavior. In particular, there is a region where one might expect spontaneous ordering $[3.0<\gamma<\gamma_s(\kappa,L)]$ which in fact exhibits a two-stage growth process in the absence of a nucleating site, and domain growth from a nucleating site (as opposed to spinodal decomposition) if one is provided.

Figure 13 shows the amplitude as a function of time for $\gamma=3.05$ for a system which is initially disordered and in which we have not supplied any strong nucleating sites. There are clearly two different stages of growth. In the first stage the amplitude grows very slowly for a long time. Then the system abruptly orders, very quickly reaching the equilibrium value. If instead we supply the system with nucleating sites at the beginning of the simulation it orders much more quickly, with domains growing from the nucleating sites. These observations are consistent with the presence of a free energy barrier that decays with time.

The free energy barrier can be identified as resulting from the free energy of the orientational order. There is a time dependent quadratic term in the free energy due to the distortion. The distortion energy is proportional to κq^2 [see Eq. (1)] so that one has an effective term

$$\mathcal{F}_d \propto \kappa q^2 L_{def}(t)^{-2} \ln[L_{def}(t)/a], \tag{41}$$

using Eq. (27) with $L_{def}(t)$ being the separation between defects. As a result, not only does the state at $\gamma=3.0$ remain

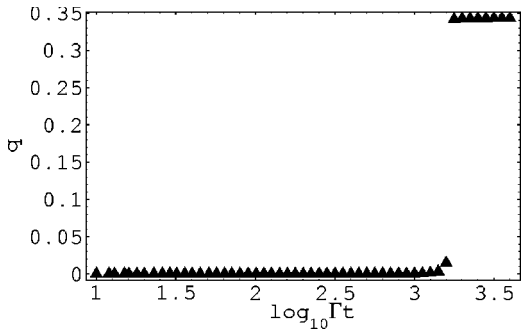

FIG. 13. Amplitude q versus time for a quench to $\gamma=3.05$. The initial fractional noise on q ($\sim 10^{-6}$) is very small and cannot cause ordering by nucleation and growth.

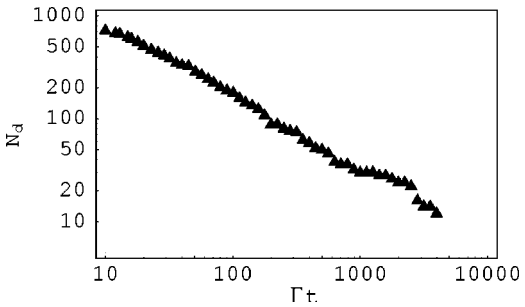

FIG. 14. Number of defects versus time for a quench to $\gamma=3.05$.

metastable but the global free energy minimum at $q>0$ may not be a minimum at zero time. This contribution to the free energy is included in Fig. 12 for different values of L_{def}.

The domain growth in the nucleated case is now easily understood. Why there is eventually ordering with no nucleation sites still requires some explanation. Equation (41) gives the average free energy contribution from the orientational order. However, locally there are regions where there is higher orientational order so that some gain in free energy can be made by increasing q in these regions. These regions are still not large enough to gain sufficiently from this to pay for the cost of an interface between fully ordered and disordered states so the elastic energy suppresses the growth in q, keeping its typical value very small. However, as we have already pointed out in Eq. (35) the diffusion constant for the orientational ordering is independent of q, as long as $q>0$. Hence the orientational ordering can proceed. (See, for instance, the number of defects as a function of time shown in Fig. 14.) As the orientation proceeds, L_{def} grows and eventually the free energy barrier is small enough that the system can form a sufficiently large region of the amplitude ordered phase to nucleate growth. Once such a region is formed the amplitude ordering can proceed rapidly.

VII. SUMMARY AND DISCUSSION

To summarize, we have used a lattice Boltzmann algorithm to investigate the phase ordering of liquid crystals quenched from the isotropic to the nematic phase. The system is described by the Beris-Edwards equations of liquid crystal hydrodynamics. These are written in terms of a tensor order parameter which means that the dynamics of topological defects that drives the phase ordering appears naturally in the simulations. The liquid crystal moves toward an equilibrium described by the Landau–de Gennes free energy.

The flexibility of the numerical scheme allows an investigation into how the ordering process is affected by the model parameters. In particular, we find that if the length scale defined by the size of the topological defects is taken to be too short the cores are pinned by the lattice as the simulation proceeds giving an incorrect value for the growth exponent. This is likely to have been the problem faced by other authors who consistently obtained a value less than the 1/2 expected from scaling arguments.

Averaging over 20 runs on a lattice of linear size 512 we obtained $\phi_{cor}=0.49\pm0.02$, $\phi_{el}=0.485\pm0.03$, and ϕ_{def}

$=0.475\pm0.03$. The value for ϕ_{el} was fitted using logarithmic corrections. Hydrodynamic flow speeds up the ordering slightly but does not change the scaling behavior. This is reasonable because, in two dimensions, interactions between the flow vortices set up by the moving defects have the same logarithmic form as the defect-defect interactions themselves. Thus theoretical and numerical results are now in pleasing agreement.

[1] I. L. Chuang, N. Turok, and B. Yurke, Phys. Rev. Lett. **66**, 2472 (1991).

[2] I. L. Chuang, R. Durrer, N. Turok, and B. Yurke, Science **251**, 1336 (1991).

[3] A. N. Pargellis, S. Green, and B. Yurke, Phys. Rev. E **49**, 4250 (1994).

[4] R. E. Blundell and A. J. Bray, Phys. Rev. E **49**, 4925 (1994).

[5] B. Yurke, A. N. Pargellis, T. Kovacs, and D. A. Huse, Phys. Rev. E **47**, 1525 (1993).

[6] M. Zapotocky, P. M. Goldbart, and N. Goldenfeld, Phys. Rev. E **51**, 1216 (1995).

[7] J.-I. Fukuda, Eur. Phys. J. B **1**, 173 (1998).

[8] H. Imura and K. Okano, Phys. Lett. **42A**, 403 (1973).

[9] P. G. de Gennes, in *Molecular Fluids*, edited by R. Balian and G. Weill (Gordon and Breach, London, 1976), p. 373.

[10] L. D. Landau and E. M. Lifshitz, *The Theory of Elasticity*, 3rd ed. (Pergamon Press, Oxford, 1986).

[11] C. Denniston, Phys. Rev. B **54**, 6272 (1996).

[12] W. R. Osborn, E. Orlandini, M. R. Swift, J. M. Yeomans, and J. R. Banavar, Phys. Rev. Lett. **75**, 4031 (1995).

[13] V. M. Kendon, J.-C. Desplat, P. Bladon, and M. E. Cates, Phys. Rev. Lett. **83**, 576 (1999).

[14] C. Denniston, E. Orlandini, and J. M. Yeomans, Europhys. Lett. **52**, 481 (2000).

[15] C. Denniston, E. Orlandini, and J. M. Yeomans, Phys. Rev. E **63**, 056702 (2001).

[16] A. N. Beris and B. J. Edwards, *Thermodynamics of Flowing Systems* (Oxford University Press, Oxford, 1994); A. N. Beris, B. J. Edwards, and M. Grmela, J. Non-Newtonian Fluid Mech. **35**, 51 (1990).

[17] P. G. de Gennes and J. Prost, *The Physics of Liquid Crystals*, 2nd ed. (Clarendon Press, Oxford 1993).

[18] J. P. Straley, Phys. Rev. A **10**, 1881 (1974).

[19] P. D. Olmsted and C.-Y. David Lu, Phys. Rev. E **56**, 55 (1997); **60**, 4397 (1999).

[20] M. Doi, J. Polym. Sci., Polym. Phys. Ed. **19**, 229 (1981); N. Kuzuu and M. Doi, J. Phys. Soc. Jpn. **52**, 3486 (1983); M. Doi, Faraday Symp. Chem. Soc. **18**, 49 (1983); M. Doi and S. F. Edwards, *The Theory of Polymer Dynamics* (Clarendon Press, Oxford, 1989).

[21] J. Feng, C. V. Chaubal, and L. G. Leal, J. Rheol. **42**, 1095 (1998).

[22] P. C. Hohenberg and B. I. Halperin, Rev. Mod. Phys. **49**, 435 (1977).

[23] S. Chen and G. D. Doolen, Annu. Rev. Fluid Mech. **30**, 329 (1998); R. Benzi, S. Succi, and M. Vergassola, Phys. Rep. **222**, 145 (1992).

[24] I. M. Lifschitz, Zh. Éksp. Teor. Fiz **42**, 1354 (1962) [Sov. Phys. JETP **15**, 939 (1962)]; S. M. Allen and J. W. Cahn, Acta Metall. **27**, 1085 (1979).

[25] A. J. Bray, Adv. Phys. **43**, 357 (1994).

[26] P. D. Olmsted and P. M. Goldbart, Phys. Rev. A **46**, 4966 (1992).

[27] A. P. Y. Wong, P. Wiltzius, R. G. Larson, and B. Yurke, Phys. Rev. E **47**, 2683 (1993).